JOURNAL OF THEORETICAL AND APPLIED MECHANICS
61, 2, pp. 219-232, Warsaw 2023
https://doi.org/10.15632/jtam-pl/159728

INVESTIGATION OF THE PAD STIFFNESS EFFECTS ON THE INITIATION OF BRAKE SQUEAL PHENOMENON

Akif Yavuz, Osman Taha Sen
Istanbul Technical University, Department of Mechanical Engineering, Istanbul, Turkey
e-mail: yavuza15@itu.edu.tr (corresponding author); senos@itu.edu.tr

The main objective of this study is to investigate pad stiffness effects on the instability of a nonlinear brake squeal model. Hence, a nonlinear mathematical model is developed. The nonlinear model is linearized to check the system stability through complex eigenvalue analysis. The results of linear stability analyses are compared to the numerical solution of the nonlinear model, and it is observed that the dynamic behavior predicted by the linear stability analysis is in accordance with the numerical solutions. Though, a discrepancy may occur at the predicted squeal frequencies with both approaches, especially at high pad stiffness levels.

Keywords: disc brake squeal, mode coupling phenomenon, linear stability analysis, nonlinear dynamics

1. Introduction

A wide variety of noise and vibration problems are observed in automotive disc brake systems. In the traditional classification, these problems are classified based on dominant frequencies as shown in Fig. 1 (Stojanovic *et al.*, 2022). Though, a phenomenological classification is also given in the literature, where the problems are classified based on physical mechanisms such as forced vibrations, vibrations primarily due to friction characteristics, and resonance effects (Jacobsson, 2003).

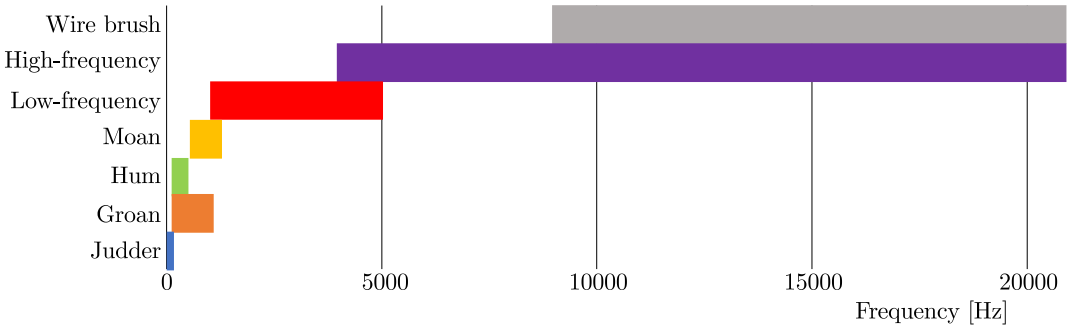

Fig. 1. Traditional classification of brake vibration and noise problems (Stojanovic *et al.*, 2022)

High frequency brake squeal noise has become an important vehicle comfort problem, even if it does not affect driving safety. Since the problem is in high frequency bands, these vibrations spread in the form of acoustic modes leading to brake noise problem (Kinkaid *et al.*, 2003). Although the problem of interest has been studied for nearly a century, and an extensive literature exists; a general solution to the brake squeal problem that can be applied to all automotive brake systems has not yet been developed (Papinniemi *et al.*, 2002). It is known that some proposed models are only suitable for certain systems and even in these systems they cannot always detect

the problem definitively. This is mainly due to the fact that the squeal phenomenon is mainly governed by friction which is not fully understood. Therefore, the mechanisms that cause the brake noise problem has not been adequately examined and the problem is still open to research.

The underlying physics leading to high frequency brake squeal noise is usually attributed to the resonance phenomenon, i.e., the natural frequency of the brake system is excited by nonconservative friction forces through several physical mechanisms; thus the system becomes dynamically unstable. In general, these physical mechanisms are defined as follows: 1) Stick-slip phenomenon with negative damping; 2) Sprag-slip phenomenon; 3) Self-excited vibrations with a constant friction coefficient; 4) Splitting or coupling of vibration modes; 5) Hammering (Kinkaid *et al.*, 2003).

In the existing literature, a wide variety of low order linear and nonlinear mathematical models are available, which are proposed for brake squeal investigation. In one study by Wang *et al.* (2014), the authors investigated squeal instability through numerical solutions of a four degree of freedom nonlinear disc brake system model. The results showed that the pad stiffness and disc velocity had significant effects on the initiation of squeal instability due to nonlinear effects of friction characteristics and contact loss. In another paper by Li *et al.* (2016), the authors developed a nonlinear mathematical model of a mass-sliding belt system and investigated the effects of preload and nonlinear contact stiffness on squeal instability. The authors observed that the surface separation between the mass and the sliding belt significantly altered the effects of preload and contact stiffness. In the study by Ghorbel *et al.* (2020), the validity of linear stability analysis was investigated through a two degree of freedom disc brake system model. The authors examined the effects of gyroscopic factors, damping and pad geometry via linear stability analysis, and obtained time domain solutions through numerical solutions of their nonlinear model. Consequently, the authors obtained a good match between the results of linear stability analysis and numerical solutions. In another study by Dakel and Sinou, where linear stability analysis was utilized, mode coupling instability was numerically investigated with a four degree of freedom system that exhibited friction nonlinearity (Dakel and Sinou, 2017). The linear stability analysis was carried out on through complex eigenvalue analysis of linearized governing equations, and the Hopf bifurcation points as a function of the kinetic friction coefficient were determined. Hochlenert used a linear stability analysis approach on a twelve degree of freedom disc brake model and investigated effects of the friction coefficient and disc angular velocity on stability of the system (Hochlenert, 2009). The author observed that the effect of the friction coefficient on dynamic instability vanished at high disc angular velocity and the effect of disc angular velocity disappeared at a high friction coefficient. Kang investigated the effect of friction coefficient characteristics on squeal instability on a two degree of freedom mathematical model (Kang, 2018). The author assumed a smooth friction-velocity curve (Stribeck type) and observed that the dynamic response of the system depended significantly on friction-velocity curve characteristics. Hoffmann *et al.* (2002) investigated the mode coupling instability through a two degree of freedom model by a time-series response and complex eigenvalue analysis.

Furthermore, the linear stability analysis approach on the investigation of squeal behavior was found to be misleading in some studies (Liu and Ouyang, 2020; Sinou, 2010; Zhang *et al.*, 2016). Liu and Ouyang studied the dynamics of a disc brake system with a five degree of freedom mathematical model by numerical and analytical means. The authors included the effects due to contact stiffness, stick-slip and geometrical nonlinearities in their model and concluded that a nonlinear stability analysis was crucial for detection of squeal instability (Liu and Ouyang, 2020). Sinou claimed that the stability analysis performed on the linearized system provided limited information about dynamic behavior of the system. Thus, the author suggested the use of numerical solutions of nonlinear governing equations for a precise investigation (Sinou, 2010). Zhang *et al.* (2016) stated that complex eigenvalue analysis applied to linearized models may lead to misinterpretations, probably due to inherent nonlinearities that have significant

effects on dynamics of the system. In yet another study by Belhocine and Ghazaly, the authors investigated the squeal phenomenon through a finite element model of the disc brake assembly, which was experimentally validated via modal testing. The authors performed stability analysis on the model and investigate the effect of Young's modulus of brake system components on the occurrence of high frequency squeal noise (Belhocine and Ghazaly, 2016).

In this study, the squeal phenomenon is investigated mathematically while utilizing a friction model obtained through experimentation on a mass-sliding belt test setup. First, a nonlinear mathematical model is developed to investigate the effect of preload on the system. Second, the nonlinear model is linearized, and its stability is assessed through complex eigenvalue analysis for different operating conditions, which are preload and belt velocity. The values of the critical pad stiffness at which the system switches from a stable to unstable regime are determined for various operating conditions, and the effects of the preload and belt velocity on the critical pad stiffness are determined. Third, the nonlinear governing equations are numerically solved for the same operating conditions; the results are compared to the linear stability analysis. It is observed that both models exhibit similar dynamic behavior from the perspective of predicting dynamic behavior of the system. Finally, the effect of pad stiffness on surface separation at the contact interface is numerically investigated through the nonlinear model, and the performance of the linear stability analysis is assessed by comparing the calculated squeal frequencies. It is observed that an increase of pad stiffness leads to significant surface separation effects, which leads to nonlinear dynamic behavior. Thus, the squeal frequencies predicted with linear stability analysis start to deviate from the numerical solutions of nonlinear equations at high pad stiffness levels.

The key assumptions in this current study can be listed as follows: 1) Damping is ignored in the mathematical modeling since there is no significant damping in a real physical brake system. 2) The springs utilized in the mathematical model are all assumed to have linear characteristics. This is a reasonable assumption due to minor deformations observed in these springs. 3) For linearization of the governing equations, the discontinuous 'sgn' function in nonlinear governing equations is replaced with a continuous 'tanh' function. This assumption may lead to a failure, especially at solution points near the discontinuity. However, this assumption is required for the linear stability analysis. 4) The surface separation effect is also ignored in the linear stability analysis. Though, it is shown in the study that squeal frequencies determined from the linearized model start to deviate from the nonlinear model as the surface separation effect becomes significant.

A flowchart of this study is shown below in Fig. 2, where the experimental and computational findings are depicted in detail. Furthermore, the novelty of this study is the fundamental understanding of the effects of operating parameters (angular configuration, preload and belt velocity) on the critical pad stiffness and the effect of pad stiffness on the surface separation at the contact interface.

2. Nonlinear two degree of freedom mathematical model

A nonlinear two degree of freedom mathematical model is developed as shown in Fig. 3. In the model, the pad is assumed as a mass m that performs planar motion in the vertical plane without any rotation. Thus, translations in x and y directions are defined as the two degrees of freedom. Furthermore, the brake disc is defined as a translating surface at constant velocity V underneath the mass. The pad is attached to the common ground with four linear springs. The two of these springs that represent stiffness of the brake pad k_1 and k_2 are positioned with arbitrary angles θ_1 and θ_2 with respect to the horizontal axis. The other springs k_3 and k_4 are parallel to the horizontal axis, and they represent elasticity of the clips between the pad and

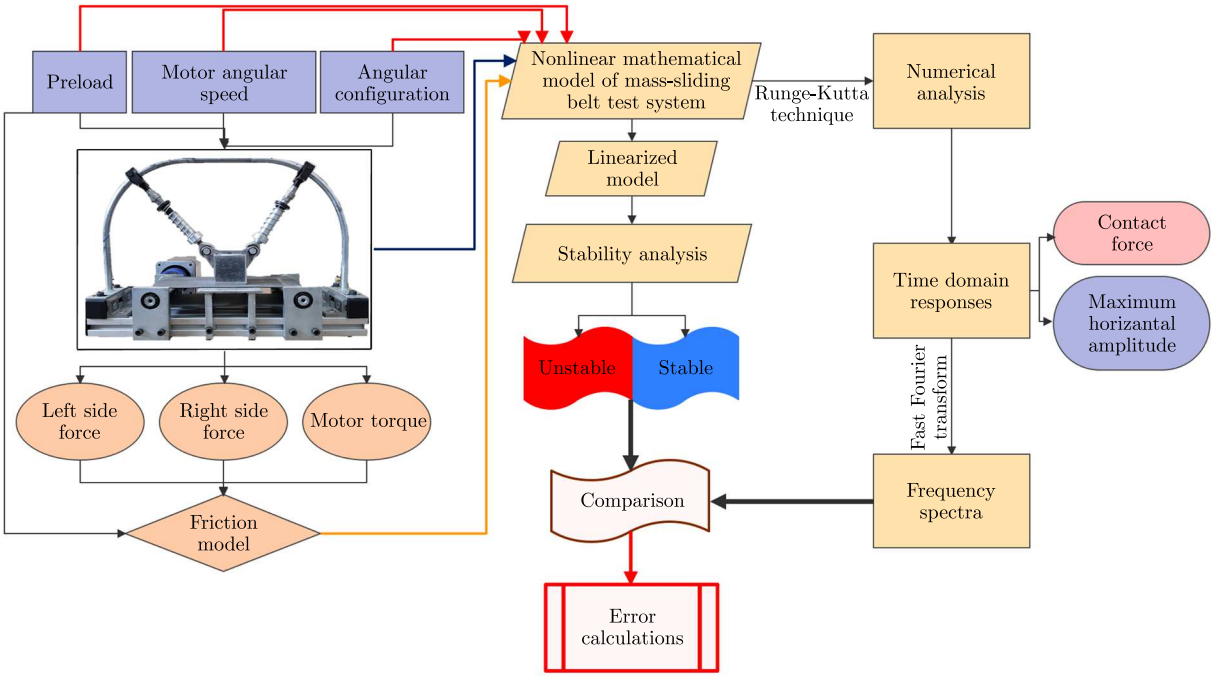

Fig. 2. The flowchart of the study

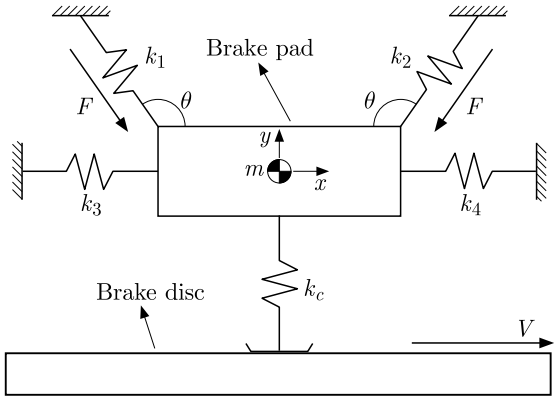

Fig. 3. Schematics of the nonlinear two degree of freedom mathematical model

the caliper. The contact between the pad and the disc is defined as a point contact where the stiffness at the contact interface is defined by another linear elastic element k_c, which can only generate a compressive force in y-direction. Furthermore, a pretension L_{pre} is defined on the contact spring k_c. The preload F is applied to springs k_1 and k_2 in order to mimic the effect of hydraulic brake pressure.

The dynamic friction coefficient μ at the pad/disc contact interface is obtained experimentally in a mass-sliding belt experiment (Fig. 4a), which has a similar structure to the model shown in Fig. 3. In this experiment, a mass is pushed on the sliding belt via two telescopic arms, which are supported by the springs k_1 and k_2, see Fig. 3. Note that the configurations of these springs are kept intact during the experiments, i.e., $\theta = (27/36)\pi$. The experiments are performed at different belt speeds and preload conditions. Restoring forces in springs k_1 and k_2 are measured with two force transducers, and the moment of the electric motor that drives the sliding belt is acquired from the inverter. Thus, the tangential force at the mass/sliding belt

interface is obtained, and the instantaneous dynamic friction coefficient $\mu_i(t)$ at the contact interface is calculated from the measured data as follows

$$\mu_i(t) = \frac{F_t(t)}{F_l(t)\sin\theta + F_r(t)\sin\theta + 2F\sin\theta} \tag{2.1}$$

where $F_t(t)$ is the instantaneous tangential force at the contact interface, and $F_l(t)$ and $F_r(t)$ are the instantaneous normal forces on the left and right telescopic arms, respectively. Furthermore, the term F is the constant preload applied to springs k_1 and k_2, respectively. In summary, the numerator in Eq. (2.1) is the tangential force at the brake pad and brake disc contact interface, which is calculated by dividing the measured motor torque by the radius of the drum. The denominator in Eq. (2.1) represents the total normal load at the brake pad and brake disc contact interface, which has a constant (due to the preload F) and time varying (due to $F_l(t)$ and $F_r(t)$) components. Though the forces F, $F_l(t)$ and $F_r(t)$ are not perpendicular to the disc surface, thus their projections on the vertical axis are calculated by multiplying these forces by $\sin\theta$.

Based on measurements, it is observed that the estimated dynamic friction coefficient $\mu_i(t)$ at a given parameter set does not alter significantly during tests. Hence, an average dynamic friction coefficient μ is defined by the mean value theorem for integrals in the closed interval of $[0, T]$ as below (Sawczuk *et al.*, 2021a,b)

$$\mu = \frac{1}{T}\int_0^T \mu_i(t)\, dt \tag{2.2}$$

Consequently, the dynamic friction coefficient is experimentally obtained as shown in Fig. 4b for two different preload levels, i.e., $F = 50\,\mathrm{N}$ and $F = 200\,\mathrm{N}$ with respect to V. Here, it should be emphasized that a two-dimensional linear regression model is utilized for derivation of the friction model depicted in Fig. 4b.

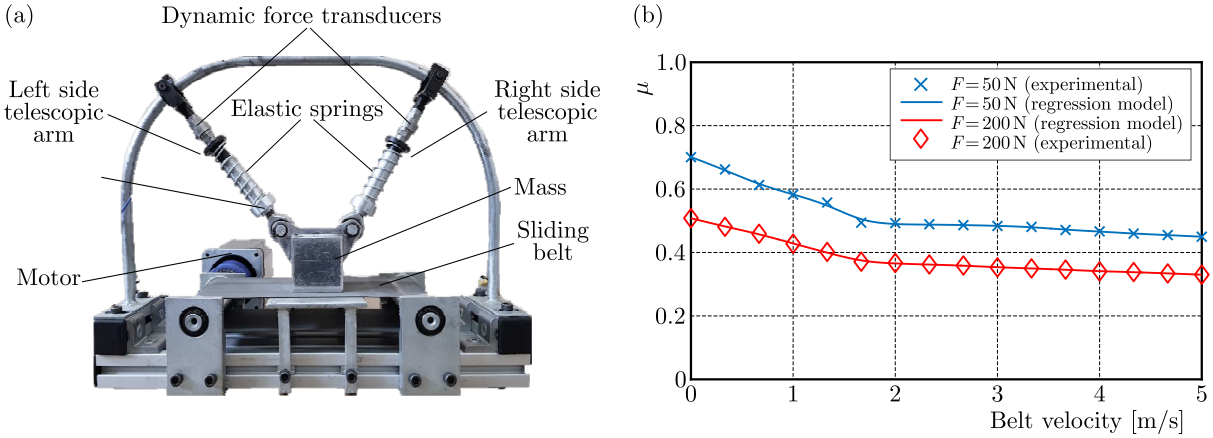

Fig. 4. (a) Mass-sliding belt test rig, (b) change of the dynamic friction coefficient with respect to V at two different preload levels

The nonlinear governing equations of the system shown in Fig. 3 are derived by calculating the elastic force vectors for each spring by Hooke's law. These force vectors are then projected on the x and y axes, and the force equilibria in these directions are obtained as shown in Eqs. (2.3)

$$
\begin{aligned}
m\ddot{x} &+ k_1 \frac{\left(\sqrt{x^2+y^2-2L_1(x\cos\theta+y\sin\theta+L_1^2}-L_1\right)(x-L_1\cos\theta)}{\sqrt{x^2+y^2-2L_1(x\cos\theta+y\sin\theta)+L_1^2}} \\
&+ k_2 \frac{\left(\sqrt{x^2+y^2+2L_2(x\cos\theta-y\sin\theta)+L_2^2}-L_2\right)(x+L_2\cos\theta)}{\sqrt{x^2+y^2+2L_2(x\cos\theta-y\sin\theta)+L_2^2}} \\
&+ (k_3+k_4)x + \frac{1}{2}k_c\mu(y-L_{pre})[1+\ \mathrm{sgn}\,(L_{pre}-y)] = 0 \\
m\ddot{y} &+ k_1 \frac{\left(\sqrt{x^2+y^2-2L_1(x\cos\theta+y\sin\theta)+L_1^2}-L_1\right)(y-L_1\sin\theta)}{\sqrt{x^2+y^2-2L_1(x\cos\theta+y\sin\theta)+L_1^2}} \\
&+ k_2 \frac{\left(\sqrt{x^2+y^2+2L_2(x\cos\theta-y\sin\theta)+L_2^2}-L_2\right)(y-L_2\sin\theta)}{\sqrt{x^2+y^2+2L_2(x\cos\theta-y\sin\theta)+L_2^2}} \\
&+ \frac{1}{2}k_c(y-L_{pre})[1+\ \mathrm{sgn}\,(L_{pre}-y)] + 2F\sin\theta = 0
\end{aligned}
\tag{2.3}
$$

The terms L_1 and L_2 in Eqs. (2.3) are the free lengths of the springs k_1 and k_2, respectively. Furthermore, the following nonlinearities are considered in the mathematical model: 1) Kinematic nonlinearity due to θ_1 and θ_2; 2) Contact loss nonlinearity due to piecewise linear 'sgn' function; and 3) Dynamic friction coefficient model μ obtained experimentally. For detailed derivation of the nonlinear governing equations, readers should refer to (Sen and Singh, 2021)

3. Linearization of the nonlinear governing equations

The stability of the system is assessed with complex eigenvalue analysis, which requires linearization of the governing equations. Consequently, the following assumptions are made in order to obtain a simplified linear mathematical model. First, the velocity of the disc is assumed to be greater than the velocity of the pad in the x direction, i.e., $\dot{x} < V$ for any time. Thus, the direction of the friction force vector does not change. Second, the pad and the disc are assumed to be in perpetual contact, i.e., $y < L_{pre}$. Third, the nonlinear terms due to the angular configuration θ in Eqs. (2.3) are linearized with Taylor series expansion around the point $(x, y) = (0, 0)$. Furthermore, the discontinuous piecewise linear 'sgn' function is approximated with a continuous 'tanh' function as $\mathrm{sgn}\,(z) = \tanh(\sigma z)$, where σ is a regularizing factor (Oberst *et al.*, 2013). Finally, the linearized equations are obtained as follows

$$
\begin{aligned}
m\ddot{x} + (K_{aa}+k_3+k_4)x + (K_{ab}+\mu k_c)y &= \frac{1}{2}\mu k_c L_{pre}[\tanh(\sigma L_{pre})+1] \\
m\ddot{y} + K_{ab}x + (K_{bb}+k_c)y &= -2F\sin\theta + \frac{1}{2}\mu k_c L_{pre}[\tanh(\sigma L_{pre})+1]
\end{aligned}
\tag{3.1}
$$

where K_{aa}, K_{ab} and K_{bb} are defined as

$$
\begin{aligned}
K_{aa} &= (k_1+k_2)\cos^2\theta \qquad & K_{ab} &= (k_1-k_2)\sin\theta\cos\theta \\
K_{bb} &= (k_1+k_2)\sin^2\theta
\end{aligned}
\tag{3.2}
$$

Using the above equations, the static equilibrium point (x^*, y^*) is obtained as

$$\begin{aligned} x^* &= \frac{1}{(K_{aa}+k_3+k_4)(K_{bb}+k_c)-K_{ab}(K_{ab}+\mu k_c)}\Big[(K_{bb}+k_c)\Big(\frac{1}{2}\mu k_c L_{pre}[\tanh(\sigma L_{pre})+1]\Big) \\ &\quad -\Big(-2F\sin\theta+\frac{1}{2}\mu k_c L_{pre}[\tanh(\sigma L_{pre})+1]\Big)(K_{ab}+\mu k_c)\Big] \\ y^* &= \frac{1}{(K_{aa}+k_3+k_4)(K_{bb}+k_c)-K_{ab}(K_{ab}+\mu k_c)}\Big[(K_{aa}+k_3+k_4)\Big(-2F\sin\theta \\ &\quad +\frac{1}{2}\mu k_c L_{pre}[\tanh(\sigma L_{pre})+1]\Big)-K_{ab}\Big(\frac{1}{2}\mu k_c L_{pre}[\tanh(\sigma L_{pre})+1]\Big)\Big] \end{aligned} \tag{3.3}$$

Finally, the linearized equations are shifted to the static equilibrium position via linear transformation $(\overline{x}, \overline{y}) = (x + x^*, y + y^*)$, and the Jacobian matrix is obtained to be used in complex eigenvalue analysis.

4. Stability analysis with complex eigenvalue solution

The stability of the system is assessed by the complex eigenvalue solution of the Jacobian matrix of the linearized model. Thus, the instability of the system is attributed to the complex eigenvalue λ with a positive real part. Particularly, the effect of preload F and disc velocity V on the instability is investigated. In the analysis, the angular configuration of k_1 and k_2 are selected to be $\theta = (27/36)\pi$ as in the experiments, and the complex eigenvalues are obtained over a broad range of brake pad stiffness levels (k_1 and k_2). Note that $k_1 = k_2$ is also assumed. The real and imaginary parts of the complex eigenvalues are depicted in Figs. 5-8 for different preload levels and disc velocities.

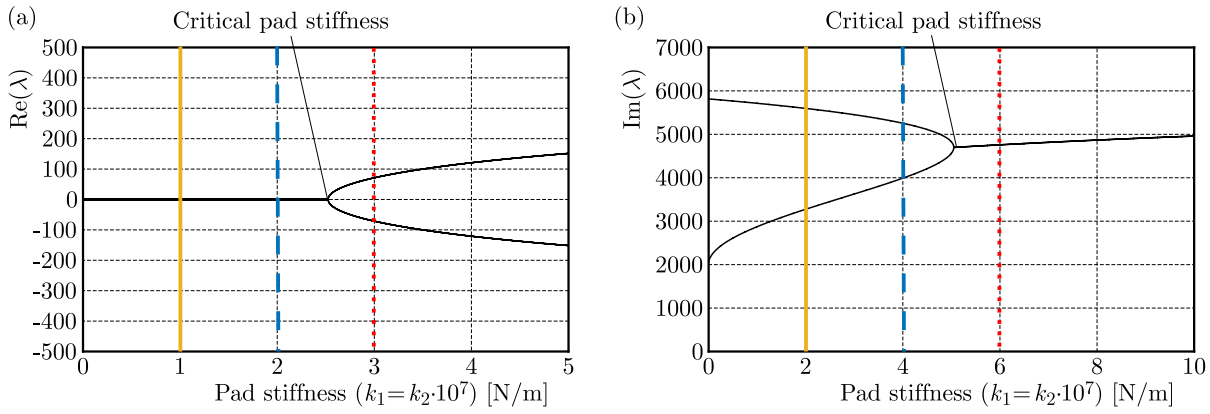

Fig. 5. Real and imaginary parts of the complex eigenvalues for $F = 50\,\mathrm{N}$ and $V = 1\,\mathrm{m/s}$: (a) Re(λ), (b) Im(λ)

As evident from Figs. 5-8, the system exhibits mode coupling behavior, i.e., the imaginary parts of the eigenvalues are coupled for one specific value of brake pad stiffness, which is called the critical pad stiffness k_{cr}, and the real part of one eigenvalue becomes positive. This dynamic behavior triggers the squeal phenomenon. Figure 5 shows the real and imaginary parts of the complex eigenvalues for $F = 50\,\mathrm{N}$ and $V = 1\,\mathrm{m/s}$. As seen in Figs. 5a and 5b, the system exhibits two purely imaginary eigenvalues up to $k_1 = k_2 = 5.16 \cdot 10^7\,\mathrm{N/m}$. Thus, $k_{cr} = 5.16 \cdot 10^7\,\mathrm{N/m}$, and the vibration modes occur at two distinct frequencies. At the point, when $k_1 = k_2 = 5.16 \cdot 10^7\,\mathrm{N/m}$, the vibration modes get coupled, and the real part of one of the eigenvalues becomes positive. Hence the system switches to an unstable state. In the second analysis depicted in Fig. 6, the value of belt velocity is increased to $V = 4\,\mathrm{m/s}$ while keeping F intact. Similarly,

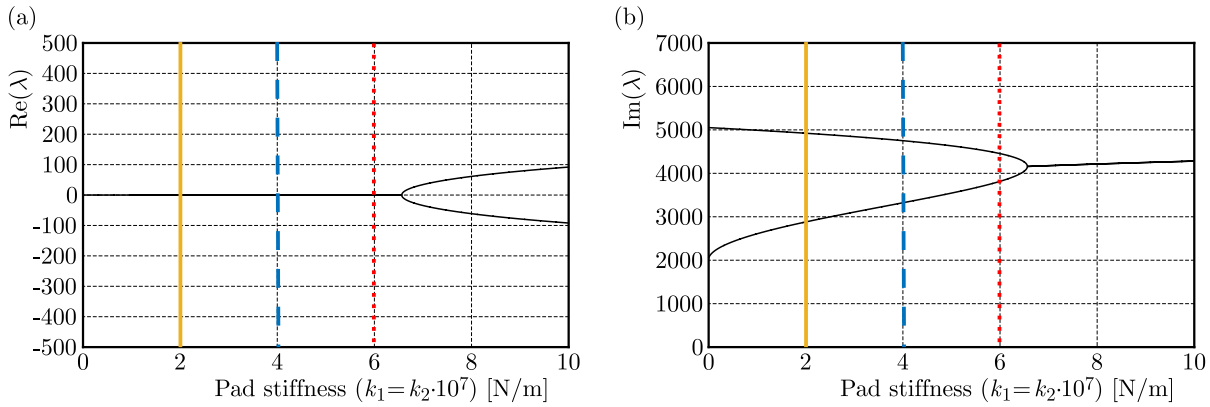

Fig. 6. Real and imaginary parts of the complex eigenvalues for $F = 50\,\mathrm{N}$ and $V = 4\,\mathrm{m/s}$: (a) Re(λ), (b) Im(λ)

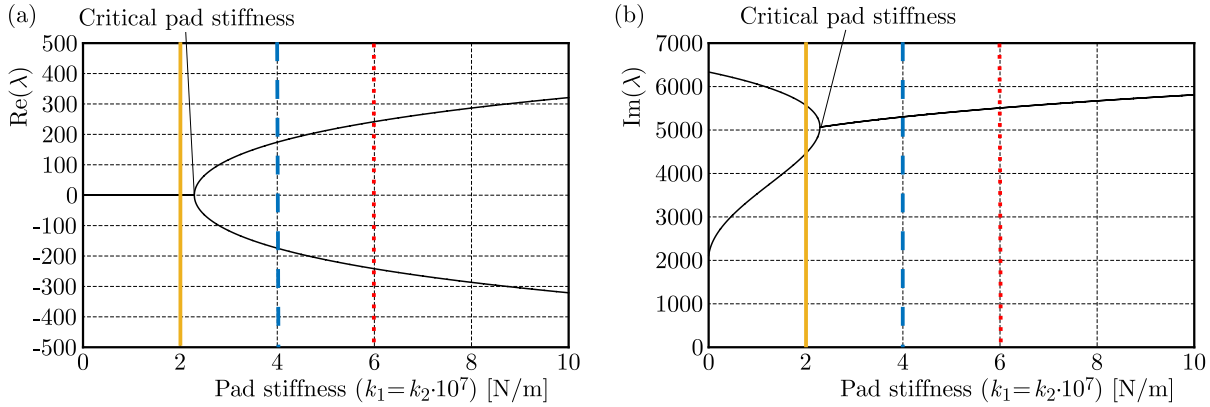

Fig. 7. Real and imaginary parts of the complex eigenvalues for $F = 200\,\mathrm{N}$ and $V = 1\,\mathrm{m/s}$: (a) Re(λ), (b) Im(λ)

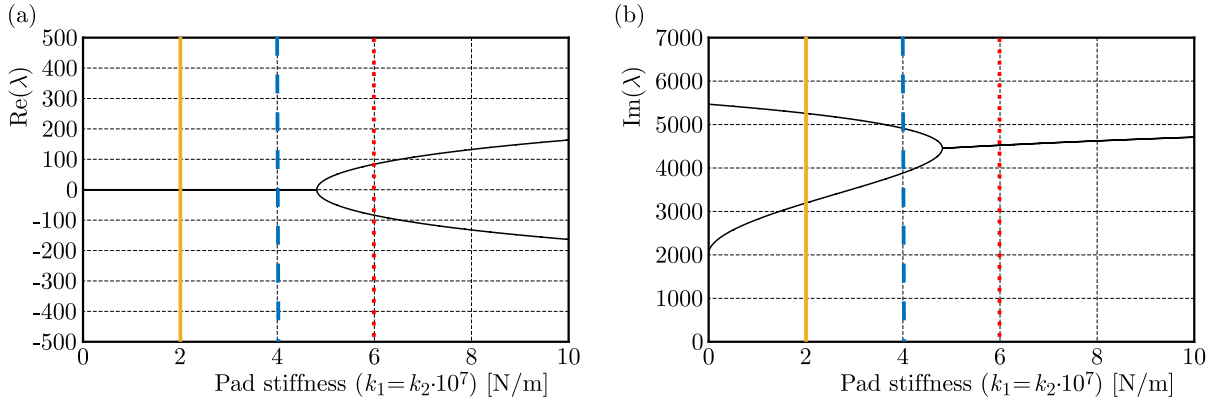

Fig. 8. Real and imaginary parts of the complex eigenvalues for $F = 200\,\mathrm{N}$ and $V = 4\,\mathrm{m/s}$: (a) Re(λ), (b) Im(λ)

the mode coupling behavior is again observed though for a higher k_{cr}, which is $6.71 \cdot 10^7\,\mathrm{N/m}$. The next analysis is run at $F = 200\,\mathrm{N}$ and $V = 1\,\mathrm{m/s}$ (Fig. 7), and it is seen that the value of k_{cr} is reduced to $2.10 \cdot 10^7\,\mathrm{N/m}$. Thus, the system is stable for the case shown with the yellow dashed line, but it performs unstable dynamics for the cases represented with blue and red dashed lines. In the last analysis (Fig. 8), which is run at $F = 200\,\mathrm{N}$ and $V = 4\,\mathrm{m/s}$ operating conditions, k_{cr} is increased to $4.97 \cdot 10^7\,\mathrm{N/m}$. Therefore, it is concluded that the increase of the preload extends the unstable regime, i.e., an increase in the preload leads to reduction in k_{cr}. On the

contrary, an increase at a given disc velocity reduces the unstable regime by increasing the value of k_{cr}.

In the next analysis, the effect of preload F on k_{cr} is investigated at two different disc velocities, and the change of k_{cr} with respect to F is depicted in Fig. 9. As seen in figures, the value of k_{cr} decreases with an increase of the preload. Furthermore, the area below the k_{cr} curves represent a stable region, and the area above the k_{cr} curves are the regions of instability. Though, at a given preload value, the critical pad stiffness value is increased with an increase of the disc velocity. Furthermore, observe the three vertical lines (solid yellow, dashed blue and dotted red) in Fig. 9, which correspond to $k_1 = k_2 = 2 \cdot 10^7\,\mathrm{N/m}$, $k_1 = k_2 = 4 \cdot 10^7\,\mathrm{N/m}$ and $k_1 = k_2 = 6 \cdot 10^7\,\mathrm{N/m}$, respectively. For the case of $V = 1\,\mathrm{m/s}$ (Fig. 9a), the preload values, where the stable/unstable regime transitions occur, are found to be 248 N, 79 N and 27 N. Note that the system is in an unstable regime when the preload is higher than the preload value where the transition occurs. Thus, for $F = 50\,\mathrm{N}$, the system exhibits unstable dynamics only for $k_1 = k_2 = 6 \cdot 10^7\,\mathrm{N/m}$. Though, the unstable dynamic behavior is observed for $k_1 = k_2 = 4 \cdot 10^7\,\mathrm{N/m}$ and $k_1 = k_2 = 6 \cdot 10^7\,\mathrm{N/m}$ when the preload is $F = 200\,\mathrm{N}$. This is also evident from vertical lines depicted in Figs. 5 and 7. For an other disc velocity $V = 4\,\mathrm{m/s}$, it is seen in Fig. 9b that unstable dynamic behavior is observed only for $k_1 = k_2 = 6 \cdot 10^7\,\mathrm{N/m}$ when the preload is greater than 128 N. Thus, for $F = 50\,\mathrm{N}$, the system is always in a stable state for the given k_1 and k_2 values. Though, when $F = 200\,\mathrm{N}$, unstable dynamic behavior is now observed. This claim is also observed from the vertical lines in Figs. 6 and 8.

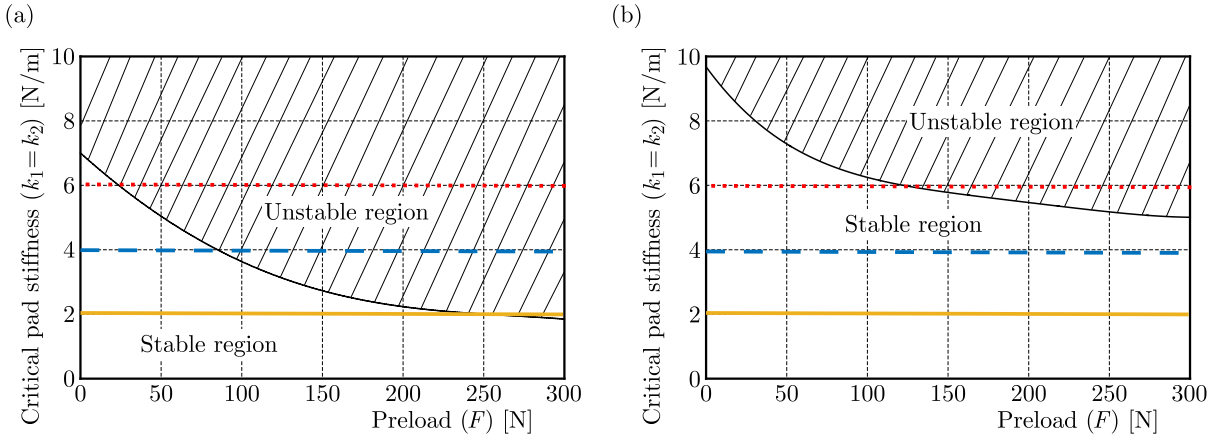

Fig. 9. The effect of preload on the critical pad stiffness: (a) $V = 1\,\mathrm{m/s}$, (b) $V = 4\,\mathrm{m/s}$

5. Numerical solution of nonlinear governing equations

In order to assess the results of linear stability analysis, the nonlinear governing equations are solved numerically with the 4th order explicit Runge-Kutta technique, and the responses in the time domain are obtained for the same operating conditions. Furthermore, the time domain responses are transformed to the frequency domain in order to assess the existence of nonlinearities. The time domain results are obtained for the three pad stiffness values of the prior analysis of Figs. 5-8, i.e., $k_1 = k_2 = 2 \cdot 10^7\,\mathrm{N/m}$, $k_1 = k_2 = 4 \cdot 10^7\,\mathrm{N/m}$ and $k_1 = k_2 = 6 \cdot 10^7\,\mathrm{N/m}$. Furthermore, the numerical results are obtained for the two preload levels, i.e., $F = 50\,\mathrm{N}$ and $F = 200\,\mathrm{N}$. The frequency spectra for these cases are shown in Figs. 10a and 10b, respectively. Note that the existence of super-harmonic peaks in the spectra are attributed to the significant contribution of nonlinearities, at which the squeal behavior is expected to occur. As seen from the spectra of Fig. 10a, the super-harmonic peaks arise only for the pad stiffness of $k_1 = k_2 = 6 \cdot 10^7\,\mathrm{N/m}$. Thus, it is claimed that it is highly possible to observe squeal behavior in

this particular case. Note that these two cases are also found to be the unstable cases in Figs. 5 and 9a. Increasing the preload to 200 N (Fig. 10b) makes the super-harmonic peaks emerge also for $k_1 = k_2 = 4 \cdot 10^7$ N/m. Thus, $k_1 = k_2 = 4 \cdot 10^7$ N/m case also now becomes a candidate at which the squeal occurrence is highly possible. Observe that these results are again coherent with the results of linear stability analysis depicted in Figs. 7 and 9a. Therefore, it is seen that similar dynamic behavior is observed with both stability analysis of the linearized model and numerical solutions of the nonlinear governing equations.

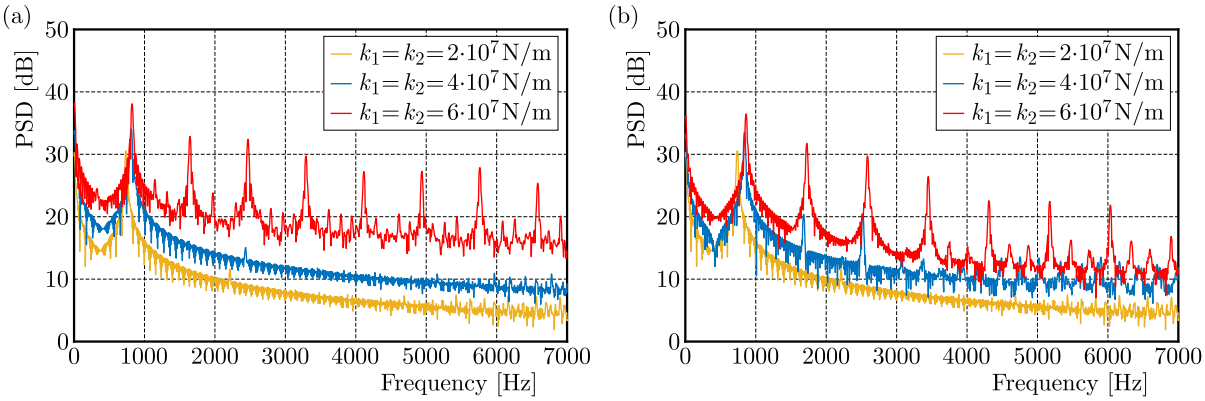

Fig. 10. Frequency spectra obtained from the numerical solutions of nonlinear governing equations for $V = 1$ m/s: (a) $F = 50$ N, (b) $F = 200$ N

Note that the linear stability analysis is based on the assumption of perpetual contact between the pad and disc surfaces. Though, the nonlinear governing equations consider the surface separation effect. In order to understand the effect of this simplification on the performance of linear stability analysis, squeal frequencies are obtained with both approaches for different pad stiffness values, and they are tabulated in Table 1. Here, the analysis is carried out for $F = 300$ N in order to guarantee squeal occurrence.

Table 1. Comparison of linear and nonlinear model results in terms of the squeal frequency ($V = 1$ m/s and $F = 300$ N)

Pad stiffness $k_1 = k_2$ [N/m]	Squeal frequency [Hz]		Error [%]	Contact loss duration [s]
	Nonlinear model	Linear model		
$2 \cdot 10^7$	964	958	0.62	0
$4 \cdot 10^7$	1095	1083	1.09	2.17
$6 \cdot 10^7$	1148	1119	2.52	3.02
$8 \cdot 10^7$	1302	1241	4.68	3.97
$10 \cdot 10^7$	1682	1538	8.56	5.79

Errors listed in Table 1 are the absolute percentage errors of squeal frequencies obtained via linear stability analysis with respect to the nonlinear model. Furthermore, the contact loss durations, which are calculated from the numerical solutions of the nonlinear governing equations, are also given in the table. Observe that the deviation between squeal frequencies increases as the value of pad stiffness increases; the same trend is also observed for the contact loss duration, which was also claimed by Aronov *et al.* (1984) based on their experimental studies. Hence, it is concluded that the performance of linear stability analysis worsens as the nonlinear effects (i.e., surface separation) dominate the dynamics of the system.

The numerically calculated time domain responses of the interfacial contact force between the brake pad and brake disc from the nonlinear model are depicted in Fig. 11 for two levels of pad stiffness. In the first case (Fig. 11a), where a smaller pad stiffness is assumed

($k_1 = k_2 = 2 \cdot 10^7\,\mathrm{N/m}$), the contact force is found to be always greater than zero. Hence, a perpetual contact is obtained at the contact interface, and the error on the predicted squeal frequencies is minimal as seen in Table 1. In the second case, the pad stiffness is set to a higher level ($k_1 = k_2 = 10{\cdot}10^7\,\mathrm{N/m}$), and it is observed that the surface separation starts to occur at the contact interface as evident from the time instances where the contact force is zero (Fig. 11b). Consequently, the deviation between the predicted squeal frequencies increases.

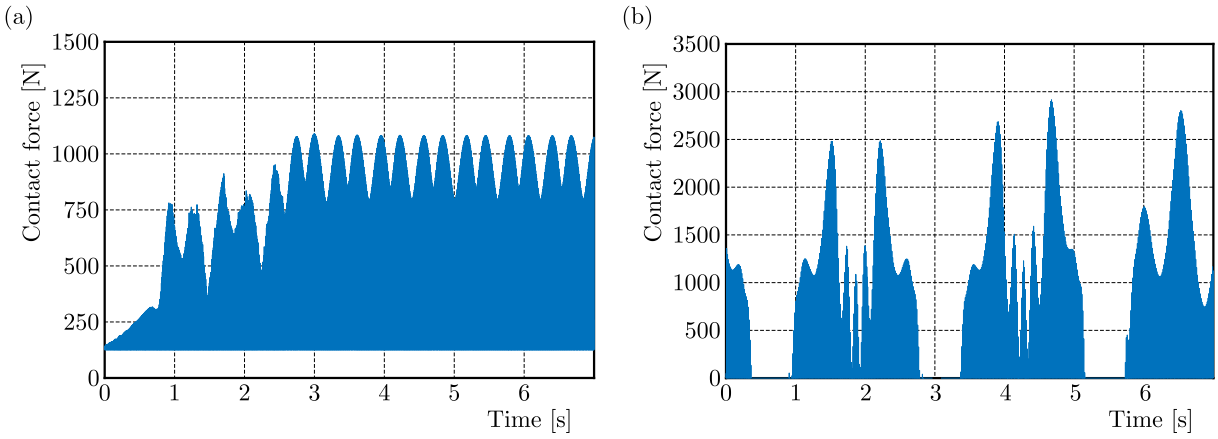

Fig. 11. Time domain results of the nonlinear model for $V = 1\,\mathrm{m/s}$ and $F = 300\,\mathrm{N}$): (a) $k_1 = k_2 = 2 \cdot 10^7\,\mathrm{N/m}$, (b) $k_1 = k_2 = 10 \cdot 10^7\,\mathrm{N/m}$

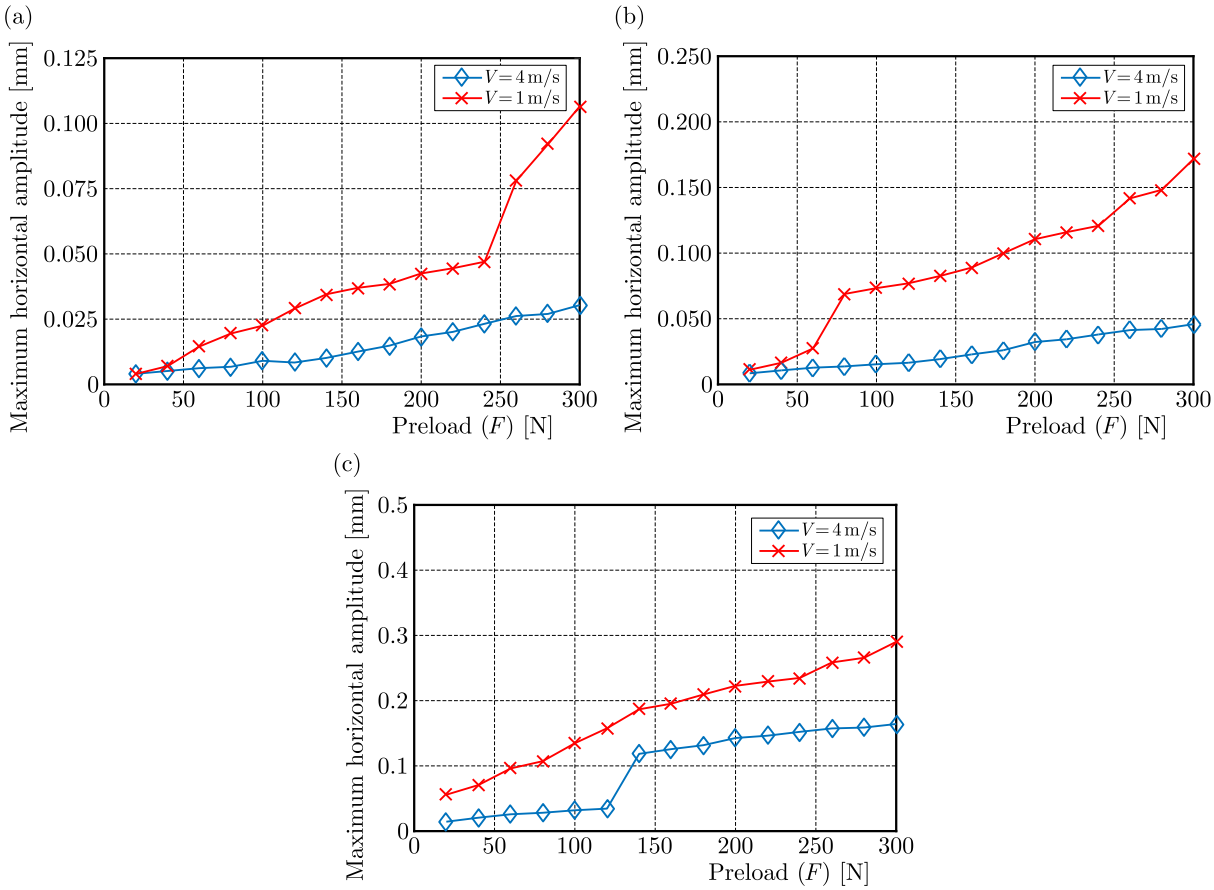

Fig. 12. Peak displacement amplitudes of the mass in x axis with respect to preload at different belt velocities: (a) $k_1 = k_2 = 2 \cdot 10^7\,\mathrm{N/m}$, (b) $k_1 = k_2 = 4 \cdot 10^7\,\mathrm{N/m}$, (c) $k_1 = k_2 = 6 \cdot 10^7\,\mathrm{N/m}$

In another analysis, numerical solutions are obtained at different preload levels for the same pad stiffness values of prior analyses. Furthermore, the results are obtained at two different levels of the disc velocity. The peak displacement amplitudes are gathered and scattered in Fig. 12. In the first case where $k_1 = k_2 = 2 \cdot 10^7\,\mathrm{N/m}$ (Fig. 12a), it is seen that the peak displacement amplitudes gradually increase for $V = 4\,\mathrm{m/s}$. Though, a sudden increase is observed around $F = 250\,\mathrm{N}$ at $V = 1\,\mathrm{m/s}$. Comparing this result with Fig. 9a, it is seen that $F = 250\,\mathrm{N}$ is at the vicinity of where the transition from the stable to unstable regime occurs. Similar results are also observed for the case of $k_1 = k_2 = 4 \cdot 10^7\,\mathrm{N/m}$ (Fig. 12b). Though, now a sudden increase in the displacement amplitude occurs around $F = 80\,\mathrm{N}$ for $V = 1\,\mathrm{m/s}$. Note that the stable to unstable regime transition occurs at $F = 79\,\mathrm{N}$ (Fig. 9a). Furthermore, the displacement amplitudes gradually increase for $V = 4\,\mathrm{m/s}$. These results are again in accordance with the results of the linear stability analysis of Fig. 9b. In the last case, where $k_1 = k_2 = 6 \cdot 10^7\,\mathrm{N/m}$ (Fig. 12c), the peak displacement amplitudes now gradually increase only for $V = 1\,\mathrm{m/s}$, while a sudden amplitude jump occurs around $F = 130\,\mathrm{N}$ for $V = 4\,\mathrm{m/s}$. As seen in Fig. 9b, this pad stiffness value is the only one where unstable dynamic behavior is observed when the preload level is greater than 128 N, and this value is close to the preload level where the jump occurs in Fig. 12c.

6. Conclusion

In this study, a nonlinear two degree of freedom mathematical model is developed for investigation of the brake squeal phenomenon with emphasis put on the brake pad stiffness. The nonlinear governing equations are linearized with further assumptions, and stability of the system is investigated by complex eigenvalue analysis. Furthermore, friction characteristics at the pad/disc contact interface are defined with a friction model derived through data obtained experimentally. Hence, the effect of pad stiffness on stability of the system is investigated for different preloads and belt velocities. Finally, the nonlinear governing equations are numerically solved for all operating conditions, and the results are compared to the linear stability analysis. Furthermore, the linear stability analysis of the predicted squeal frequencies are compared with the numerical solutions of nonlinear governing equations. Some of the major findings of this study are listed below:

- Mode coupling is found to be a significant mechanism that triggers unstable dynamic behavior and leads to the brake squeal phenomenon.
- An increase in the preload level leads to reduction of the critical pad stiffness for all disc velocities. Thus, it is concluded that the pad stiffness should be reduced at high preload conditions in order to guarantee stable dynamic behavior.
- An increase in the belt velocity leads to an increase of the critical pad stiffness for the same preload condition. Hence, the unstable region is found to be contracted as the disc velocity increases.
- The squeal frequencies obtained via linear stability analysis and from numerically calculated time histories of nonlinear governing equations are found to be similar.
- The frequency spectra calculated from time histories of the nonlinear governing equations exhibit super-harmonic peaks in the cases which are found to be unstable through linear stability analysis. Thus, it is shown that a similar dynamic response is obtained with both approaches, since the emergence of super-harmonic peaks is usually attributed to a nonlinear dynamic response.
- It is observed that the surface separation effects become significant at high pad stiffness levels.

- The predicted squeal frequencies from linear stability analysis start to deviate from the frequencies calculated from time histories of the nonlinear mathematical model as the surface separation effects become significant.
- The peak displacement amplitudes calculated numerically from the nonlinear governing equations exhibit a sudden jump at the boundaries of stable to unstable regime transition, which is attributed to the high amplitude oscillation behavior of the squeal response.

In conclusion, it is seen that the linear stability analysis successfully predicts the dynamic behavior of the system. Though the estimation of the squeal frequency may exhibit slight errors based on the strength of nonlinearity.

This study can be expanded by validating the major findings with experimentation. For example, experiments can be conducted at high pad stiffness levels, and the response of the system can be investigated experimentally. This requires the following slight modifications of the current experiment: 1) Two extra telescopic arms on both sides of the mass should be added in the experiment in order to mimic the developed mathematical model; and 2) Experiments at which different levels of spring stiffness are utilized should be performed. Though, in the current study an experimental validation is out of the scope. Thus, this validation remains as a future work.

References

1. Aronov V., D'Souza A.F., Kalpakjian S., Shareef I., 1984, Interactions among friction, wear, and system stiffness – Part 1: Effect of normal load and system stiffness, *Journal of Tribology*, **106**, 54-59
2. Belhocine A., Ghazaly N.M., 2016, Effects of Young's modulus on disc brake squeal using finite element analysis, *International Journal of Acoustics and Vibration*, **21**, 3, 292-300
3. Dakel M., Sinou J.J., 2017, Stability and nonlinear self-excited friction-induced vibrations for a minimal model subjected to multiple coalescence patterns, *Journal of Vibroengineering*, **19**, 1, 604-628
4. Ghorbel A., Zghal B., Abdennadher M., Walha L., Haddar M., 2020, Investigation of friction-induced vibration in a disk brake model, including mode-coupling and gyroscopic mechanisms, *Proceedings of the Institution of Mechanical Engineers, Part D: Journal of Automobile Engineering*, **234**, 2-3, 887-896
5. Hochlenert D., 2009, Nonlinear stability analysis of a disc brake model, *Nonlinear Dynamics*, **58**, 63-73
6. Hoffman N., Fischer M., Allgaier R., Gaul L., 2002, A minimal model for studying properties of the mode-coupling type instability in friction induced oscillations, *Mechanics Research Communications*, **29**, 4, 197-205
7. Jacobsson H., 2003, Aspects of disc brake judder, *Proceedings of the Institution of Mechanical Engineers, Part D: Journal of Automobile Engineering*, **217**, 6, 419-430
8. Li Z., Ouyang H., Guan Z., 2016, Nonlinear friction-induced vibration of a slider-belt system, *Journal of Vibration and Acoustics (ASME)*, **138**, 4, 041006
9. Liu N., Ouyang H., 2020, Friction-induced vibration considering multiple types of nonlinearities, *Nonlinear Dynamics*, **102**, 20572075
10. Kang J., 2018, Lyapunov exponent of friction-induced vibration under smooth friction curve, *Journal of Mechanical Science and Technology*, **32**, 8, 3563-3567
11. Kinkaid N.M., O'Reilly O.M., Papadopoulos P., 2003, Automotive disc brake squeal, *Journal of Sound and Vibration*, **267**, 105-166

12. Oberst S., Lai J.C.S., Marburg S., 2013, Guidelines for numerical vibration and acoustic analysis of disc brake squeal using simple models of brake systems, *Journal of Sound and Vibration*, **332**, 2284-2299

13. Papinniemi A., Lai J.C.S., Zhao J.Y., Loader L., 2002, Brake squeal: A literature review, *Applied Acoustics*, **63**, 391-400

14. Sawczuk W., Cañás A.M.R., Ulbrich D., Kowalczyk J., 2021a, Modeling the average and instantaneous friction coefficient of a disc brake on the basis of bench tests, *Materials*, **14**, 16, 4766

15. Sawczuk W., Ulbrich D., Kowalczyk J., Merkisz-Guranowska A., 2021b, Evaluation of wear of disc brake friction linings and the variability of the friction coefficient on the basis of vibroacoustic signals, *Sensors*, **21**, 17, 5917

16. Sen O.T., Singh R., 2021, Dynamics of a simplified nonlinear model offering insights into the hammering type brake squeal initiation process, *Noise Control Engineering Journal*, **69**, 3, 243-261

17. Sinou J.J., 2010, Transient non-linear dynamic analysis of automotive disc brake squeal – On the need to consider both stability and nonlinear analysis, *Mechanics Research Communications*, **37**, 96-105

18. Stojanovic N., Belhocine A., Abdullah O.I., Grujic I., 2022, The influence of the brake pad construction on noise formation, people's health and reduction measures, *Environmental Science and Pollution Research*, 1-12

19. Wang H., Liu X., Shan Y., He T., 2014, Nonlinear behavior evolution and squeal analysis of disc brake based on different friction models, *Journal of Vibroengineering*, **16**, 5, 2593-2609

20. Zhang Z., Oberst S., Lai J.C.S., 2016, On the potential of uncertainty analysis for prediction of brake squeal propensity, *Journal of Sound and Vibration*, **377**, 123-132

Manuscript received October 24, 2022; accepted for print December 12, 2022